Journal of Bio- and Tribo-Corrosion (2020) 6:99
https://doi.org/10.1007/s40735-020-00391-6

Effect of TiO_2 Thin Film Coating on AZ91D Alloy and Investigation of Corrosion Behavior, Mechanical Properties, and Biocompatibility

M. Samiee[1] · Z. S. Seyedraoufi[1] · Y. Shajari[2] · M. J. Eshraghi[2]

Received: 25 March 2020 / Revised: 19 May 2020 / Accepted: 1 July 2020 / Published online: 21 July 2020
© Springer Nature Switzerland AG 2020

Abstract

Today magnesium and its alloys have applications in different industries and in addition to this they are used as orthopedic implants. Some of the magnesium alloys can be used as biodegradable implants in the body. Coating of the ceramic material on the magnesium alloys is one of the methods to increase the lifetime of these alloys. In this research, TiO_2 thin film was coated on the surface of the AZ91D using the sputtering method. Morphology and cross-section of the coating were done using Field emission scanning electron microscopy (FESEM), X-ray diffraction analysis (XRD), Vickers hardness test (VM), roughness testing (RT) to investigate the properties of corrosion, polarization tests of corrosion in a simulated body fluid (SBF), adaptability of the sample in the body environment from the toxicity assessment test (MTT) and cellular adhesion. Results from the corrosion test show that the corrosion rate of the coated samples with TiO_2 is improved compared to the samples without coating. The percentage of cell survival on the surface of the samples was increased from 80% for the uncoated sample to 90% for the coated sample with TiO_2, and the hardness of the coated sample was 119 Hv, and its roughness was 0.12 µm. Applying the coating by increasing the hardness and real contact area and reducing the friction coefficient can increase the wear resistance of the substrate.

Keywords Thin films · Corrosion · TiO_2 · Wear · Biomedical applications

1 Introduction

Magnesium and its alloys are commonly used in different industries due to their strength because of the high strength-to-weight ratio [1]. Today, magnesium and its alloys have many application in the field of air-space and transportation industries as well as orthopedic implants. Some magnesium alloys are also used as biodegradable implants in the body and reduce the number of painful surgeries among patients [2]. In recent years, alloys based on cobalt, nickel, and titanium are used for this purpose. However, these materials needed a second surgery to remove the implants after improvement. Mechanical strength is another disadvantage of these materials that lead to disequilibrium at the interface tension of the implant and tissue and impairs the natural growth of human bone [3, 4]. But magnesium and its alloys have more mechanical suitability with human bone and can facilitate the improvement. Magnesium is not toxic for the human body and solution of some amount of magnesium around the tissue does not lead to inflammation, and it is also necessary for bone growth and its improvement [5, 6].

AZ91D has the solid matrix solution of α-Mg with the dendrite structure, and brittle phase of β-$Mg_{17}A1_{12}$ are distributed in the grain boundary. Magnesium and its alloys have some major disadvantages [7]. These disadvantages impede more application of magnesium alloys in the industry. The most important of these disadvantages are high reactivity and meager resistance to corrosion. Undesirable wear behavior is another disadvantage of these alloys that limits the application of contact load [8–10]. These features are some reasons for not using the magnesium alloys in some specific cases. The coating is one of the most effective ways to reduce corrosion and to increase the surface properties. Different methods are used for this purpose, some of which are conversion coating, sol–gel, precipitate from the vapor phase, including CVD, PVD, cold spray, and platting [11–16]. Due to the high hardness, corrosion resistance and biocompatibility of TiO_2, the use of TiO_2

✉ M. Samiee
mohsen_samiee1993@yahoo.com

[1] Department of Materials Engineering, Karaj Branch, Islamic Azad University, Karaj, Iran

[2] Materials and Energy Research Center, 31787-316 Karaj, Iran

coating along with the lightweight preservation of the implants seems to increase the wear and corrosion resistance and biocompatibility of magnesium implants. Since few studies have been done in this field so far, this research could be the beginning of great progress in the implant manufacturing industry.

Since magnesium alloys have a high-medical potential, additional operations that reduce the challenges of using magnesium in the body are effective in developing their usage as implants. In this study, it is tried to improve the electrochemical, biocompatibility, and abrasion properties of this alloy using TiO_2 biocompatible coating on the surface of AZ91D alloy so that this material can be used more easily as an implant.

2 Experimental Procedures

2.1 Sample Preparation

In this research, AZ91D magnesium alloy was used as a substrate. Chemical composition of AZ91D magnesium alloy obtained using atomic emission spectroscopy (AES) has been shown in Table 1. Samples with dimensions of 10 mm × 10 mm × 2 mm were cut using a microcutter.

Before applying the coating, first, the samples were polished with the sandpaper and then were micro-polished for 10 min with felt carpet. Then based on the ASTM D2651 standard, they went under the operation of deoiling and deoxidization [17]. Then film deposition of the samples was done using sputtering method by the radio frequency magnetic sputtering device RF, with the basic pressure in the layer container of 10^{-7} mbar and the film deposition of the TiO_2 coating was done using working pressure of about 2.5×10^{-3} mbar with the charge of 25 cm3/min under the argon gas for 15 min.

2.2 An Investigation of the Microstructure and Mechanical Properties

Since surface topography and morphology can significantly affect the corrosion and also the cellular adhesion, we used an emission scanning electron microscopy (FESEM) model MIRA3 manufactured by the TESCAN equipped with EDS to investigate the microstructure of the sample. To provide microscopic images of the cross-section areas, all stages of metallurgical preparation, including sanding and polishing, were performed. To detect phases and chemical composition, we used the X-ray diffraction (XRD) device model PW 1800 manufactured by the PHILIPS company with Fielmann nickel, radiation of Cu kα and a maximum working voltage of 30 kV. The hardness of the coating was measured using a Vickers microhardness testing model (AMSLERD-6700) by applying 50 g weight for 20 s. Mentioned microhardness for every sample was measured five times on average. To measure the surface roughness, we used MAHR roughness tester made in Germany. Wear test on the coated and uncoated was done under the weight of 4 N and on the distance of 1000 m with the method of the pin on disk. For the abrasive pin, steel wearisome 52,100 was used with the hardness of 59 HRC. The wear test was used with a slip rate of 0.1 m/s. Changes were reported every 100 m. The worn surface was investigated using scanning electron microscope (SEM) manufactured by the TESCAN. In the Fig. 1, the schematic of pin on disk wear test has been shown.

2.3 Electrochemical Corrosion Resistance

Corrosion behavior of the samples in a simulated body fluid (SBF) was investigated using potentiostat/galvanostat EG&G at the temperature of 37 °C. Each of the samples were closed on the cell as working electrodes and platinum electrode, and saturated calomel electrode was used as a reference, and counter electrodes were used to experiment. Potentiodynamic polarization curve was determined after 90 min immersion in about − 250 to 2000 mv with the sweep velocity of 1 mV/s. pH was set by HCI and TRIS at 7.4. Table 2 shows the ion concentration in the SBF solution.

2.4 In Vitro Test

To test the cellular toxicity process and cellular proliferation, we used the cellular line MG63 (NCBI C555) from

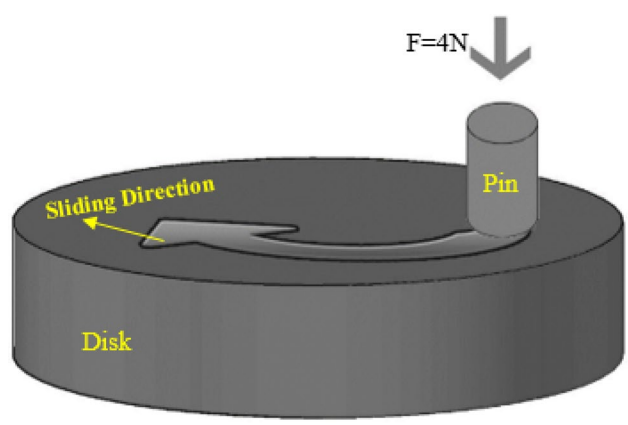

Fig. 1 Schematic of pin on disk wear test

Table 1 Chemical composition of the AZ91D alloy based on the weight percentage

Cu	Fe	Mn	Ni	Zn	Al	Mg	Others
0.03	0.005	0.35	0.002	0.5	9.7	Bal	0.002

Table 2 Ion concentration in the SBF solution (mM) [18]

Ion	Cl^-	HCO_3^-	Mg^{2+}	K^+	HPO_4^{2-}	Ca^{2+}	Na^+	SO_4^{2-}
SBF	147.8	4.2	1.5	5	1	2.5	142	0.5

the Pasteur Institute in Iran. This cell comes from human type cells and the Sarcoma decease. Also, it has both fibroblast morphology and bone texture. Based on the sample size, we used a cell culture plate with 24 wells. DMEM was used as the cell culture environment to which we added %10 of fetal bovine serum. At first, 1 ml of serum was poured into the given wells, then the coated sample with TiO_2 and uncoated sample were put into the wells before sterilization. After making sure of the full immersion in the culture environment and correct placement of the samples to cover the maximum space from the bottom of the wells, 30,000 cells with 1 ml culture environment containing the serum were added to the wells. One well without sample and containing the same amount of cell was considered as a negative control. Samples and cells were kept for 72 h in the 5% CO_2 incubator with the relative moisture of 98%, and the temperature of 37 °C. Morphology of the cells on the surface of the samples was investigated after three days of culture using fluorescence microscope with DAPI lens. To do this research, 72 h after the contact of the samples, cells and the cultural environment we emptied the culture environment and the cells were removed from the sterilize conditions of the culture plate and transferred to another plate to do the process of cell stabilization. Glutaraldehyde 2.5% was used for the stabilization process. First, the samples were washed twice with the sterilized buffer. Then each sample was kept in 2 ml of Glutaraldehyde solution for 1.5 h. After removing the samples from Glutaraldehyde solution, the samples were washed with the phosphate buffer and dehydrated using ethanol at concentrations of 60, 70, 80, 90 and 100%, respectively. Samples were respectively in 2 ml of the alcohol solutions for 5 min and at the end were kept in 100% alcohol for 10 min. After dehydration, the level of humidity in the surface was removed from the air, and samples were kept at the temperature of 4 °C until testing [18].

2.5 Toxicity Assessment Test (MTT)

The amount of proliferation and MG63 cellular viability on the surface of the samples were assessed by the toxicity assessment test (3-[4,5-dimethylthiazol-2-yl]-2,5-diphenyltetrazolium bromide (MTT)). For the same reason, 20 µl of MTT solution with the concentration of 5 mg/ml was added to the wells containing the sample and negative control. Four hours after the incubator, we emptied the culture environment, and 200 µl of DMSO was replaced. Ten min is enough to dissolve the formed color crystals, and after 10 min, 200 µl of the solution was removed from each well and kept in the cell culture plate with 96 wells and optic absorption of the wells was done by the Elisareader (Boi Tek, Elx808, and the USA) at the wavelength of nanometers. To estimate the relative cells viability in contact with the negative control of the samples, we used Eq. (1). In this equation, Ac is the absorption of negative control and As is the absorption of the sample [19].

$$\% \text{ viability} = \text{As} / \text{Ac} \times 100 \quad (1)$$

3 Results and Discussion

3.1 An Investigation of the Microstructure

Figure 2 shows the X-ray diffraction of the TiO_2 coating applied on the magnesium substrate. In the general sense, it is reported that AZ91D alloy is made of two phases of α-Mg and β-$Mg_{17}A1_{12}$ [20]. As it is shown in Fig. 2, there are two main phases of α-Mg and β-$Mg_{17}A1_{12}$, so the process of film deposition of nanoparticles of titanium on the magnesium substrate leads to the formation of Mg_2TiO_4 and $MgTi_2O_5$ phases. These spinels and middle phases are formed in the interface and substrate. As the temperature in the upper atomic layers increases locally, these intermetallic compounds are expected to form in accordance with a temperature-based diffusion mechanism.

Precipitates in the AZ91D magnesium alloys were observed by the researchers [21, 22]. The microstructure of the sample includes a matrix phase of primary α with dendrite boundaries and eutectic phases $(\alpha+\beta)$ with layer structure, and coarse particles of the phase are in that. With the film deposition of TiO_2 on the magnesium substrate, nanoparticle of titanium dioxide was formed on the substrate. Figure 3 shows the image of the FESEM morphology of the coating. Given the form of the cracks, it is obvious that they are formed because of the substrate contraction during the coating process due to the tensile stress of the coating and this leads to the cracks in the upper parts of the coating.

Figures 4 and 5 show the cross-section after applying the coating by the Sputtering method. The image of the surface morphology shows that the TiO_2 layer is distributed as the formed precipitation made of the uniform grains and the formed perceptions are dense and no condition such as a crack of observed. Previous research indicates the significant role of the uniform coating in resisting the corrosion [23, 24]. Given the ceramic nature of these coatings, any

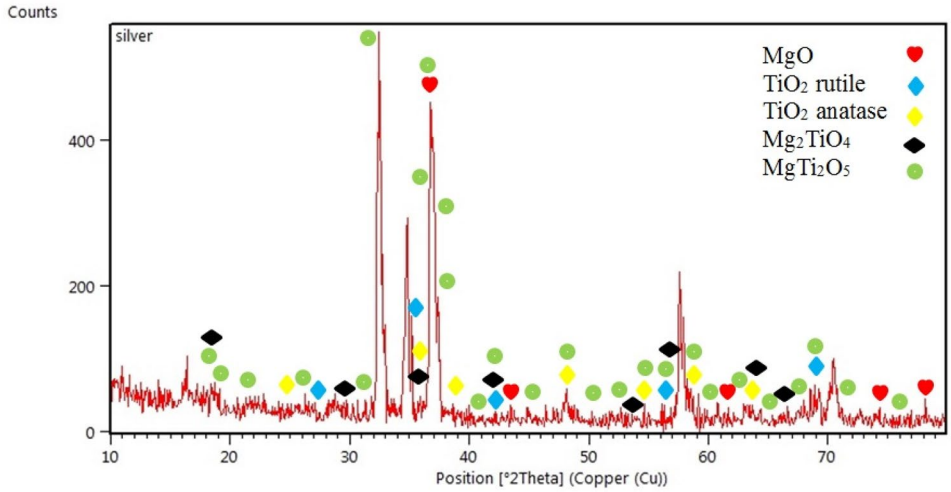

Fig. 2 X-ray diffraction of the coated sample

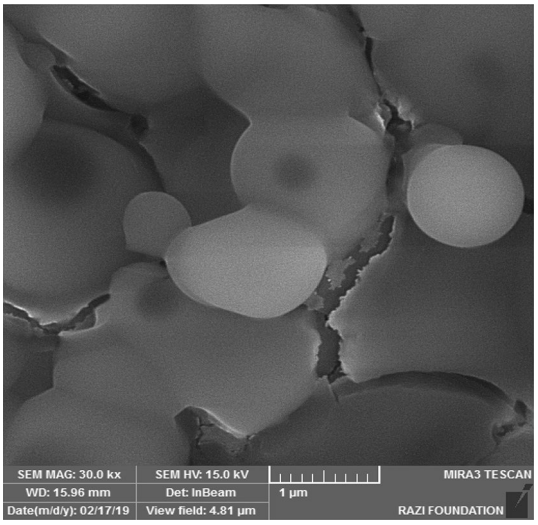

Fig. 3 FESEM image of the coated sample

type of crack and porosity decreases the surface properties and finally can remove and destroy the coating. According to Fig. 5, the biggest formed coating is 700 nm. Since the thickness of the coating has a significant effect on the surface properties of the coatings, it seems that the size of the formed coating is suitable.

According to Fig. 5, the starting point of the analysis is bottom to up. At the initial thickness, the magnesium is high, and it decreases when it is near the substrate. In the 670 and 750 µm, there are 1–2% of TiO_2 into the structure due to diffusion. At 837 µm that is the interface of the matrix and coating, this amount of magnesium increases, and the amount of TiO_2 is reduces. At points 918 and 999 µm, the amount of magnesium reaches the maximum level, and the amount of TiO_2 reaches the minimum possible amount since it has reached the surface of the coating.

3.2 Hardness and Roughness Test

Mean roughness on the surface (R_a) for both coated and uncoated sample were measured using the roughness tester, and it was observed that the roughness of the coated sample was 0.12 µm and the uncoated sample was 0.15 µm. Higher roughness on the uncoated sample helps the adhesiveness of the coating on the substrate. It seems that surface roughness contributes to adhesion of the coating by increasing the germination points of the coating and forming mechanical locks. Formation of the TiO_2 coating also decreases the roughness of the coated sample relative to the uncoated sample [25]. The hardness of the coated surface is more than the hardness of the uncoated surface due to the presence of the titanium dioxide. Obtained hardness for the coated sample and uncoated sample is 119 and 87 Hv, respectively. Figure 6 shows the bar graph of hardness and roughness before and after coating, and Table 3 presents the statistical calculations in Fig. 6.

3.3 Wear Test

Most of the in vivo implants are exposed to wear, so it is essential to study them. Figure 7 shows the trend of changes for lost weight in the wear test. As it is evident, resistance to substrate wear (AZ91D) is improved by applying a thin layer of TiO_2. Applying the TiO_2 ceramic coating has also reduced the friction coefficient. A reduction of friction coefficient and an increase of the hardness has increased resistance to wear. Meanwhile, as it was mentioned in the previous section, applying the coating reduces roughness of the surface, and this means an increase of the actual contact area. An increase in the actual contact area naturally reduces the applying tension during the wear test, and this increases the resistance to wear. SEM image shows the worn out surface of the substrate of the deep scratch and large galling that

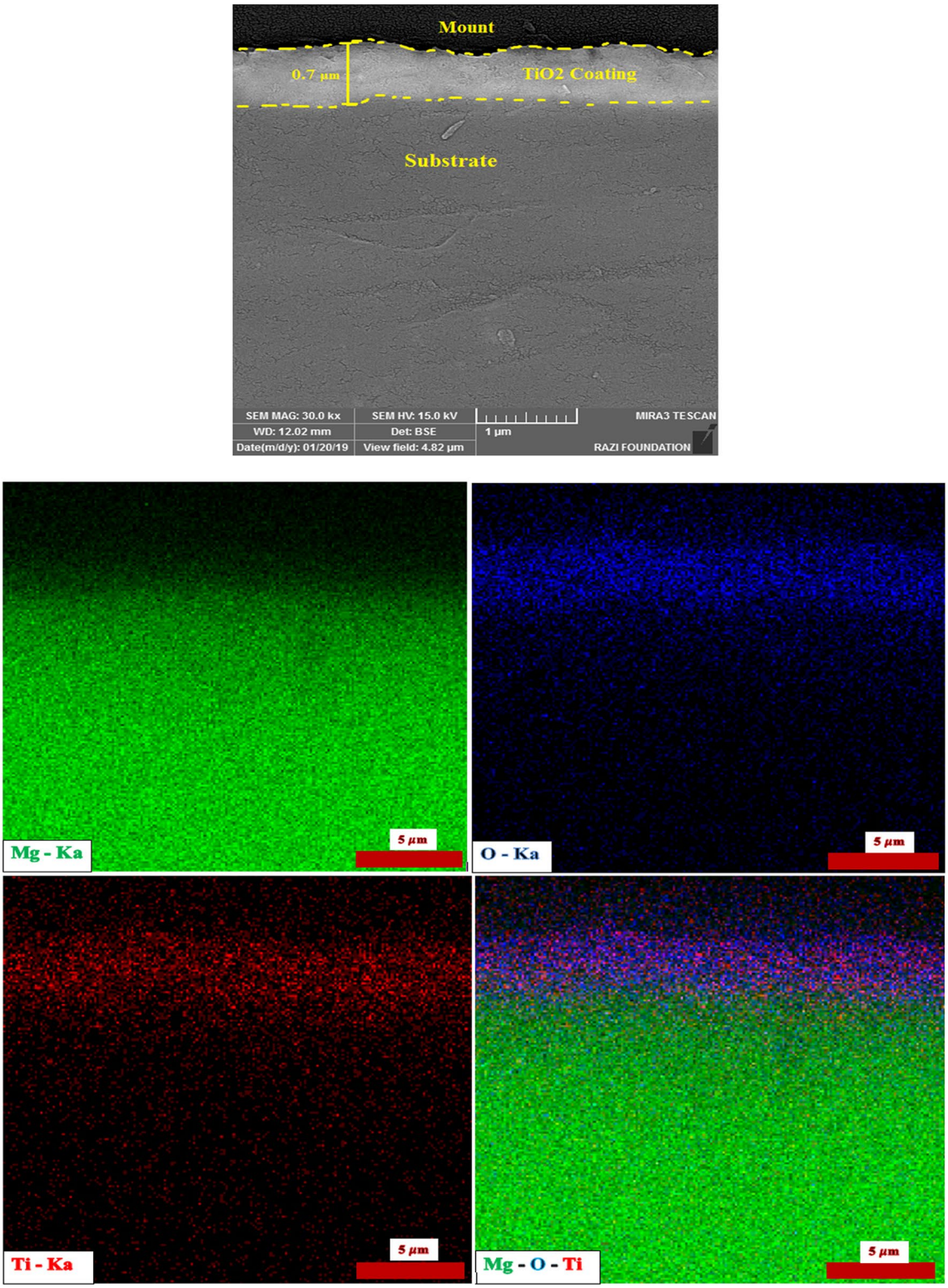

Fig. 4 FESEM image of the cross-section with the MAP analysis

happen as the result of the abrasive wear. In Fig. 7, there is some light oxide area that results from an increase in the sample temperature due to the friction during the wear test. So the dominant wear mechanism can be considered strong scratch wear. In the SEM image of worn surface of substrate, the crater regions caused by abrasive wear are seen. In fact,

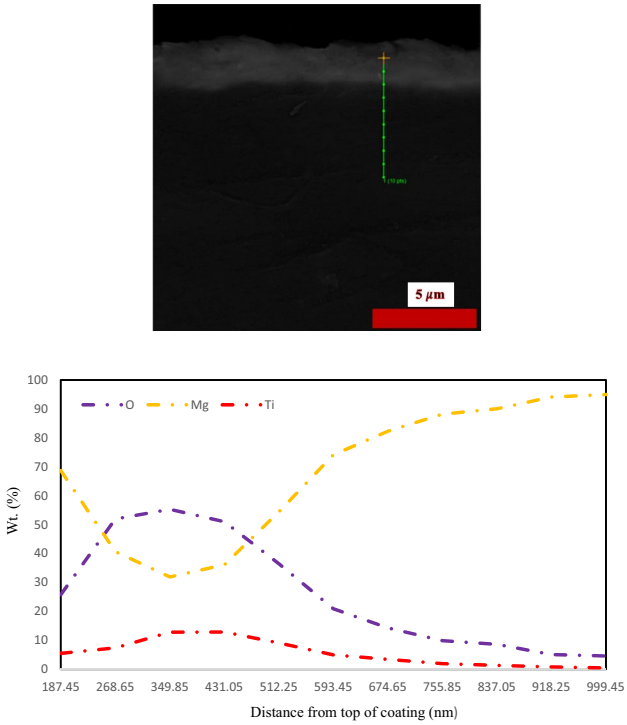

Fig. 5 FESEM image of the cross-section with the EDS analysis

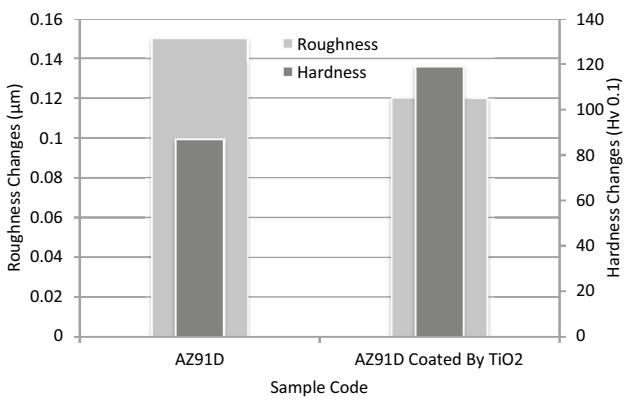

Fig. 6 Roughness and hardness changes

Table 3 Statistical information related to Fig. 6

Sample	Test	Mean	SD	*p* value
Uncoated	Hardness ($n=5$)	87 H.v	1.22	0.0
	Roughness ($n=5$)	0.15 µm	0.003	
Coated	Hardness ($n=5$)	119 H.v	1.87	0.0
	Roughness ($n=5$)	0.12 µm	0.004	

during dry sliding wear test, a brittle layer is created that areas of this brittle layer are removed due to local work hardening and high brittleness because of severe wear regime. However, Fig. 7 shows less wear scratches. This results from the reduction of the applied tension and as mentioned before the reason can be an increase in the hardness. Therefore, the formation of coating leads to the transition of the abrasive wear mechanism from severe to mild.

Due to the high coefficient of friction of the uncoated sample, after 100 m, an oxide layer is formed on the surface, which acts as a protective layer and leads to a temporary reduction of the coefficient of friction and wear rate. Due to the brittle nature of this layer, after heating the substrate and expanding it under the shear stress of the pin, it is separated from the surface in pieces and leads to an increase in the wear rate and coefficient of friction. The separated surface fragments become wear particles, leading to the wear of two objects to several objects, exacerbating scratching wear mechanism.

3.4 The Behavior of Electrochemical Corrosion

Implants in the body are under the influence of external cellular fluids, so it is necessary to investigate the corrosion behavior of these materials. Figure 8 shows the polarization curves of the coated and uncoated samples in the SBF solution. Improvement in the behavior of the polarization curve with its transfer is toward the more positive potentials and less current density [26]. Kinetic of the chemical oxidation or reduction is always controlled by a part of the process with the least rate and formed coating prevents electrochemical reactions and somehow destruction of the magnesium substrate by impairing the electron transfer on the surface. Anode and cathode reactions are as follows:

Anode reactions:

$$Ti \rightarrow Ti^{4+} + 4e \tag{2}$$

$$Ti + 2H_2O \rightarrow TiO_2 + 4H^+ + 4e^- \tag{3}$$

$$Ti^{4+} + 4H_2O \rightarrow Ti(OH)_4 + 4H^+ \tag{4}$$

$$Ti(OH)_4 \rightarrow TiO_2 + 2H_2O \tag{5}$$

Cathode reactions:

$$4H_2O + 4e^- \rightarrow 4H_2 + 4OH^- \tag{6}$$

According to Fig. 8, it is observed that with applying the coating of TiO_2, the polarization curve moves toward the more positive potentials and less current densities. According to the extracted results, the coated sample is more resistant to the corrosion compared to the substrate without coating that proves the suitable coating of the substrate. This is also clear in the polarization curves, and the current density corrosion of the coated sample is reduced compared to the

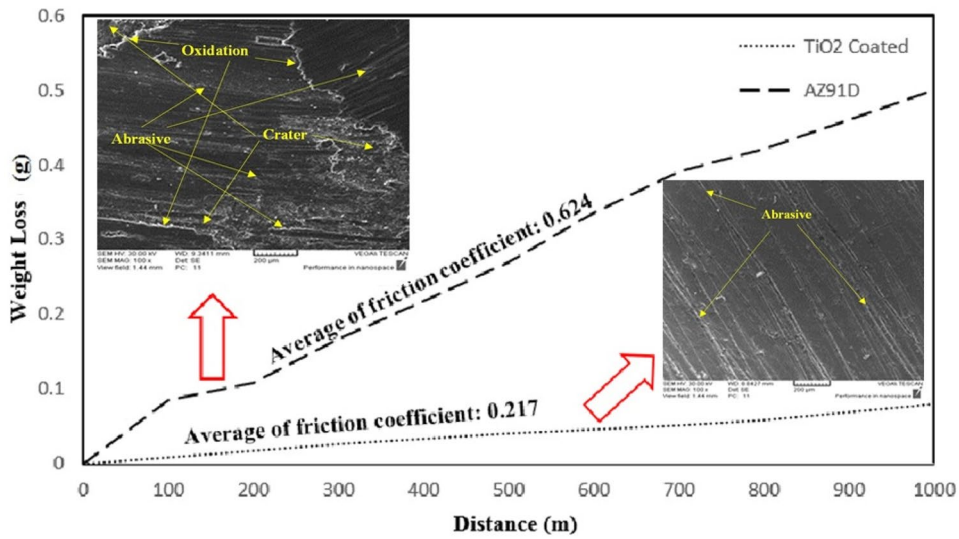

Fig. 7 Diagram of weight reduction for the samples during the wear test based on the distance with the SEM image of wear surface

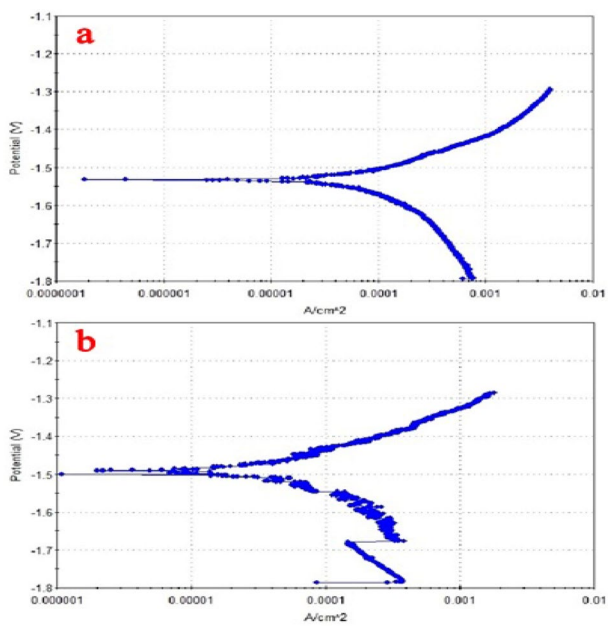

Fig. 8 Polarization curve of the samples in the SBF solution at 37 °C: **a** uncoated sample, **b** coated sample with TiO_2

uncoated sample. According to the Fig. 8, extracted data from the polarization curves, including current density corrosion (i_{corr}) and corrosion potential (E_{corr}), are shown in Table 4. As it is observed, the potential of the corrosion without coating is much more negative than the coated samples (− 1.532 V), which becomes more positive by applying the coating and in coating samples reaches to − 1.491 V that is increased by 0.041 V. Meanwhile, current density corrosion of the substrate is decreased as a result of the coating process. TiO_2 coating has more positive potential and less current corrosion compared to the uncoated sample. This

Table 4 Average of current corrosion density in the SBF solution at 37 °C

Sample	Corrosion potential E_{corr} (V)	Corrosion flow density I_{corr} (μA/cm^2)	Corrosion rate CR (mm/y)
Uncoated sample	− 1.532	4.765×10^{-3}	0.348
Coated sample	− 1.491	5.604×10^{-5}	0.269

result can happen due to the oxide ceramic layers (passive) that make the coating more resistant to corrosion [27]. Since this diagram is for the covered sample, it is more likely to prevent load transfer in this sample. On the other hand, this sample required more time to reach the equilibrium potential of the open circuit, while the immersion time of both samples in the solution before the start of the corrosion test was constant, so more noise is observed in the coated sample.

3.5 Investigation of Toxicity and Biocompatibility of the Samples

Figure 9 shows the adhesiveness, growth, broadening, morphology of the MG63 cells on the samples after 1 and 8 days of culture. Figure 9 indicates that cells are well expanded on the surface of the two samples, and the cells stick to each other and the matrix material by secretions of the microcellular such as filopodia, except that percentage of proliferation and adhesiveness of the cells on the surface of the coated sample with TiO_2 is much more than the proliferation and the adhesiveness of the cells on the uncoated sample. On the one hand, broadening of the cells on the surface of the sample coated with TiO_2 by false legs, remarkably covered most of the surface; on the other hand, on the surface of the uncoated sample, there are some parts without a cell.

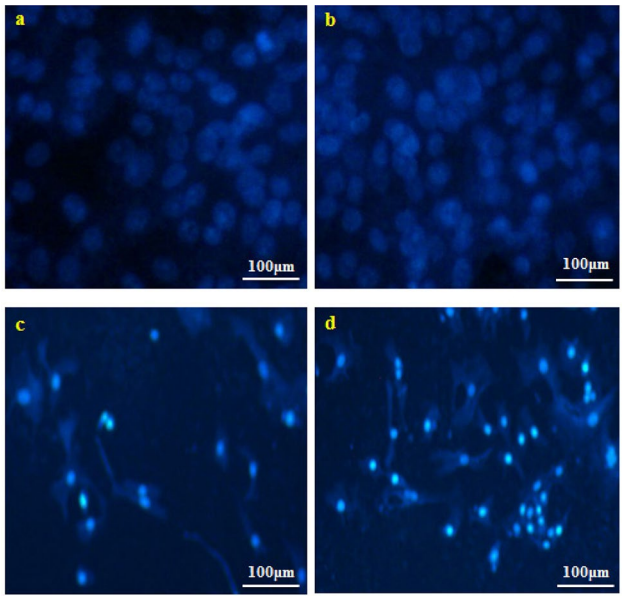

Fig. 9 Image of the cultured samples with fluorescence microscope: **a** uncoated samples for 1 day, **b** coated samples with TiO_2 for 1 day, **c** uncoated samples for 8 days, **d** coated samples with TiO_2 for 8 days

These results lead to an increase in the biocompatibility of the substrate after the coating.

Figure 10 shows the biocompatibility of the MG63 cells for 1 and 8 days in the extraction solution with the dilution of 100%, 75%, 50%, and 25% of the uncoated and coated samples with TiO_2. According to the standard ISO 10,993–5:2009, reduction of the cellular biocompatibility lower than 70% is considered the toxicity effect [20]. Given the biocompatibility of higher than 80% in all the samples in extraction solution with the dilution of 100%, 75%, 50%, and 25% for 1 and 8 days, it is possible to say that all the samples are biocompatible and in the Table 5 explained statistical calculations of Fig. 10.

As it is observed, the percentage of viability among the MG63 cells on the surface of the samples increased from 75% in uncoated sampled to 77% in the coated samples with TiO_2 after 1 day and increased from 80% in uncoated sampled to 89% in the coated samples with TiO_2 after 8 days. According to Fig. 11, it is observed that by applying TiO_2 coating, the amount of cells excitation and biocompatibility has increased and the response of the osteoblast changes remarkably with the surface changes [28–30].

Given the qualitative nature of the experiment, it can be concluded that the presence of TiO_2 not only did not inhibit cell proliferation but also significantly increased cell proliferation compared to the control sample. Biological molecules, such as soluble proteins, also provide the ability to bind chemically to titanium and magnesium ions, and encourage reactions that lead to the formation of new tissue in the body by systematic and local mechanisms.

4 Conclusion

Obtained results from this research are as follows:

Table 5 Statistical information related to Fig. 10

Sample	Day	Mean (%)	SD	*p* value
Uncoated	1 day ($n=4$)	79.25	3.09	0.031
Coated	1 days ($n=4$)	90.5	6.19	
Uncoated	8 day ($n=4$)	82.5	3.87	0.037
Coated	8 days ($n=4$)	96.5	8.22	

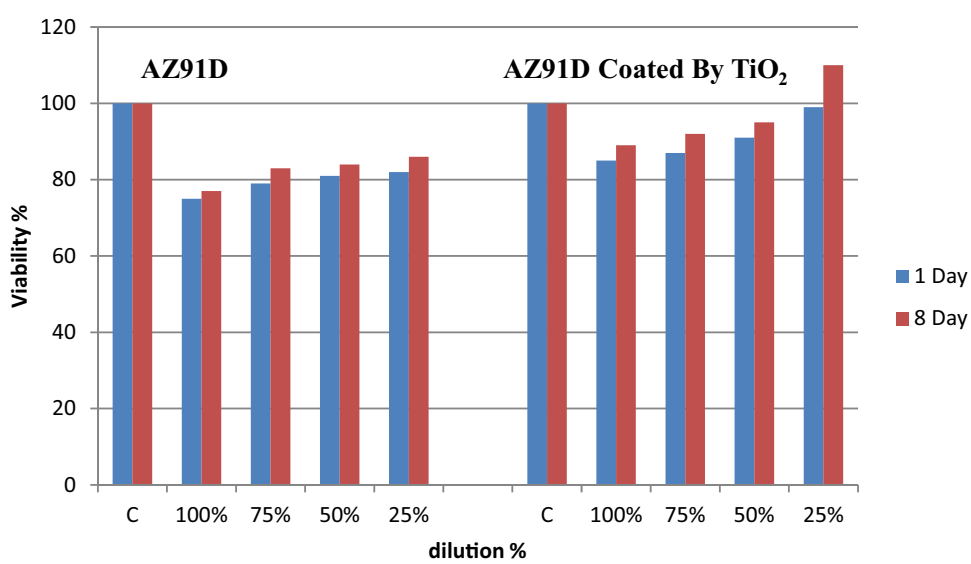

Fig. 10 Amount of biocompatibility in the osteoblast cells in the extraction solution with the dilution of 100%, 75%, 50%, and 25%: a uncoated sample, b coated sample with TiO_2

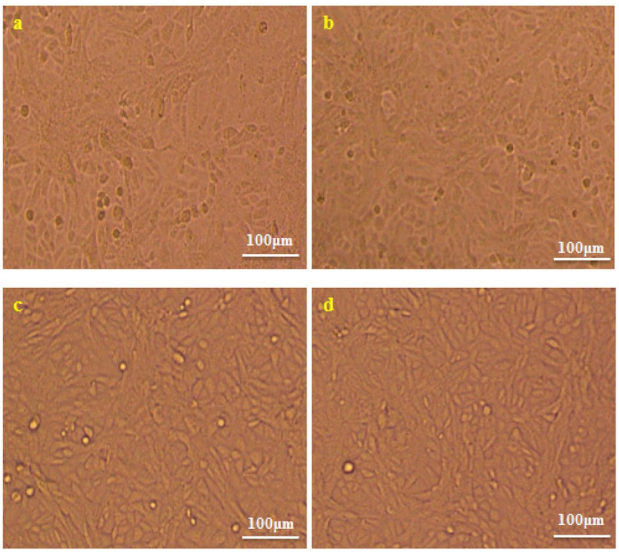

Fig. 11 Image of inverted microscope for live cells: **a** uncoated AZ91D sample after 1 day, **b** coated AZ91D sample with TiO_2 after 1 day, **c** uncoated AZ91D sample after 8 days, **d** coated AZ91D sample after 8 days

1. The method of magnetic sputtering created a thin film of TiO_2 coating effectively and without non-coherence on the surface of the AZ91D alloy.

2. An investigation of the results from the XRD analysis after coating shows that except magnesium as the substrate and TiO_2 as coating, peaks related to the $MgTi_2O_5$ and Mg_2TiO_4 is also coated in the structure.

3. Coated samples have a higher resistance to corrosion relative to the uncoated samples that show the chemical stability of the samples in the physiological environment of the body and improvement of the surface properties. The coating of TiO_2 reduces the density of the current corrosion.

4. Result of the in vivo analysis shows that the cells on the surface of the coated sample are usually perfectly broadened after 8 days. So, improvement of the biocompatibility, adhesiveness, and proliferation of the bone cells on the surface of the coated samples shows that they are good examples for implant applications.

5. Applying the TiO_2 ceramic coating has also reduced the friction coefficient. A reduction of friction coefficient and an increase of the hardness has increased resistance to wear. This can change the abrasive wear mechanism from sever to mild.

Author contributions All authors contributed to the study conception and design. Material preparation, data collection and analysis were performed by [Mohsen Samiee], methodology [Mohammad Javad Eshraghi], resources [Zahra Sadat Seyed Raoufi] and, review and editing [Yazdan Shajari]. The first draft of the manuscript was written by [Mohsen Samiee] and all authors commented on previous versions of the manuscript. All authors read and approved the final manuscript.

Funding This research did not receive any specific grant from funding agencies in the public, commercial, or not-for-profit sectors.

Compliance with Ethical Standards

Conflict of interest The authors declare that they have no known competing financial interests or personal relationships that could have appeared to influence the work reported in this paper.

References

1. Zhao M, Liu M, Song G, Atrens A (2008) Influence of the β-phase morphology on the corrosion of the Mg alloy AZ91. Corros Sci 50:1939
2. Radha R, Sreekanth D (2017) Insight of magnesium alloys and composites for orthopedicimplant applications. J Magnes Alloy 5:286
3. Pogorielov M, Husak E, Solodivnik A, Zhdanov S (2017) Magnesium-based biodegradablealloys: degradation, application, and alloying elements. Interv Med Appl Sci 9:27
4. Salahshoor M, Guo Y (2012) Biodegradable orthopedic magnesium-calcium (Mgca) alloys. Materials 5:135
5. Sankara TSN, Park IS, Lee MH (2014) Strategies to improve the corrosion resistance of microarc oxidation (Mao) coated magnesium alloys for degradable implants prospects and challenges. Progress in Mater Sci 60:1
6. Zhang L, Zhang J, Chen CF, Gu Y (2015) Advances in microarc oxidation coated AZ31 Mg alloys for biomedical. Corros Sci 91:7
7. Lopeza ADF, Lehr IL, Brugnoni LI, Saidman SB (2018) Improvement in the corrosion protection and bactericidal properties of AZ91D magnesium alloy coated with a microstructured polypyrrole film. J Magnes Alloy 6:15
8. Jinxia C, Xu C, Zhiming L (2008) Effect of mechanical vibration on microstructure and properties of cast AZ91D alloy. Results Phys 11:1022
9. Yuan G, You G, Bai S, Guo W (2018) Effects of heat treatment on the thermal properties of AZ91D magnesium alloys in different casting processes. J Alloys Compd 25:410
10. Guo KW (2011) A review of magnesium/magnesium alloys corrosion and its protection. Corros Sci 2:72
11. Zhao Q, Guo X, Dang X, Hao J, Lai J, Wang K (2013) Preparation and properties of composite MAO/ECD coatings on magnesium alloy. Colloids Surf B Biointerfaces 102:321
12. Wang H, Akid R, Gobara M (2010) Scratch-resistant anticorrosion sol–gel coating for the protection of AZ31magnesium alloy via a low temperature sol–gel route. Corros Sci 52:2565
13. Hoche H, Blawert C, Broszeit E, Berger C (2005) Galvanic corrosion properties of differently PVD-treated magnesium die cast alloy AZ91. Surf Coat Tech 193:223
14. Christoglou CH, Voudouris N, Angelopoulos GN, Pant M, Dahl W (2004) Deposition of aluminium on magnesium by a CVD process. Surf Coat Tech 184:149
15. Wang Q, Spencer K, Birbilis N, Zhang MX (2010) The influence of ceramic particles on bond strength of cold spray composite coatings on AZ91 alloy substrate. Surf Coat Tech 205:50
16. Zhu L, Li W, Shan D (2006) Effects of low temperature thermal treatment on zinc and/or tin plated coatings of AZ91D magnesium alloy. Surf Coat Tech 201:2768

17. ASTM D2651-01 (2001) Standard guide for preparation of metal surfaces for adhesive bonding. West Conshohocken, PA, ASTM International
18. Hosseini SH, Mirdamadi SH, Nemati A (2016) Investigation of mechanical properties, corrosion behavior and biocompatibility of porous Ti6Al4V Scaffold for dental implant. Metal Eng 19:135
19. Tseng P, Wang Y (2006) Overcoming trastuzumab resistance in HER2-overexpressing breast cancer cells by using a novel celecoxib-derived phosphoinositide-dependent kinase-1 inhibitor. Mol Pharmacol 70:1534
20. Boby A, Pillai UTS, Pai BC (2013) Investigation on lead and yttrium addition on the microstructure and mechanical properties of AZ91 magnesium alloy. Mater Sci Tech 7:273
21. Song G, Bowles AL, John DH (2004) Corrosion resistance of aged die cast magnesium alloy AZ91D. Mater Sci Eng A 366:74
22. Song G, Atrens A, Wu X, Zhang B (1998) Corrosion behaviour of AZ21, AZ501 and AZ91 in sodium chloride. Corros Sci 40:1769
23. Mathieu S, Rapin C, Steinmetz J, Steinmetz P (2003) A corrosion study of the main constituent phases of AZ91 magnesium alloys. Corros Sci 45:2741
24. Shi Z, Song G, Atrens A (2006) Influence of anodizing current on the corrosion resistance of anodized AZ91D magnesium alloy. Corros Sci 48:1939
25. Gonzaleza EIC, Montorsia M, Mugonia C, Montorsib M, Siligardia C (2013) Improvement of the adhesion between TiO2 nanofilm andglass substrate by roughness modifications. Phys. Procedia 40:19
26. Wang L, Zhang BP, Shinohara T (2010) Corrosion behavior of AZ91 magnesium alloy in dilute NaCl solutions. Mater Des 31:857
27. Heakal FE, Fekry AM, Fatayerji MZ (2009) Influence of halides on the dissolution and passivation behavior of AZ91D magnesium alloy in aqueous solutions. Electrochim Acta 54:1545
28. Yerokhin AL, Nie X, Leyland A, Matthews A (2000) Characterization of oxide films produced by plasma electrolytic oxidation of a Ti–6Al–4V alloy. Surf Coat Tech 130:195
29. Hohn S, Virtanen S (2015) Biocorrosion of TiO2 nanoparticle coating of Ti–6Al–4V in DMEM under specific in vitro conditions. Appl Surf Sci 329:356
30. Li N, Zheng Y (2013) Novel magnesium alloys developed for biomedical application. Mater Sci Tech 29:489

Publisher's Note Springer Nature remains neutral with regard to jurisdictional claims in published maps and institutional affiliations.